Z. Phys. C – Particles and Fields 41, 375–384 (1988)

Zeitschrift für Physik C Particles and Fields

Predictions of QCD fragmentation models in e^+e^- annihilation up to $\sqrt{s}=200$ GeV

P.N. Burrows
Department of Nuclear Physics, University of Oxford, Oxford OX1 3RH, UK

Received 16 August 1988

Abstract. Results on event and single particle characteristics are presented for the three most successful perturbative QCD + fragmentation models in the c.m. energy range $12.0 \leqq W \leqq 200$ GeV. The models were optimised to describe the properties of the large sample of hadronic events obtained by TASSO at $W=35$ GeV. The energy evolution of the observables across the range spanned by the PETRA and PEP data, $12.0 \leqq \langle W \rangle \leqq 41.5$ GeV, is reasonably well described by all the models. However, for some quantities the predictions of the different models diverge at higher energies; distributions of observables are shown at c.m. energies of 93 and 200 GeV, where data are expected from the e^+e^- colliders currently under construction. The ability to describe simultaneously, with the same parameter values, hadronic event features both at PETRA/PEP and LEP/SLC energies will provide a severe test of the models. The effects of top quark production on the event properties are illustrated for a top mass of 60 GeV/c^2. Predictions are given for the rates of multijet events up to $W=200$ GeV, where $\geqq$4-jet events dominate the cross section and will form a background to events containing heavy states which decay into hadron jets.

1 Introduction

Perturbative QCD + fragmentation models [1] of the process $e^+e^- \to \gamma/Z \to$ hadrons have been tested thoroughly during the last decade of analysis of PETRA and PEP data in the energy range $12.0 \leqq \langle W \rangle \leqq 41.5$ GeV. As the severity of the tests has increased with time, the models have become more sophisticated and are constantly being updated and improved by their authors in an attempt to obtain better agreement with the data. The models contain various arbitrary parameters, both for the perturbative QCD and hadronisation schemes, which can usually be tuned to provide a good description of the data at a given energy. For example, the latest studies on jet fragmentation using the large data samples acquired at PEP at $W=29$ GeV and PETRA at $W=35$ GeV have shown [2, 3] that the current generation of models is generally rather successful in describing most features of the data at these energies. A more stringent test is to see if the models give a good representation of the data at energies other than that at which they were tuned. Unfortunately, there are only a few thousand events at each of the other main c.m. energies explored to date, namely $\langle W \rangle \sim 14$, 22 and >40 GeV, so that statistical errors are often large relative to differences between the models, especially in the tails of distributions of observables. So far, the detectors at TRISTAN have obtained only a few hundred hadronic events around 50 GeV [4], though more data are awaited.

The construction of the next generation of e^+e^- colliders is nearing completion; within the next few years SLC and LEP should provide data at the Z^0 pole, $W \sim 93$ GeV, and towards the mid 1990's LEP-2 could be supplying annihilation events up to $W=200$ GeV. There will hence be e^+e^- data spanning an energy range of roughly 200 GeV, providing an opportunity for more stringent testing of the QCD + fragmentation models.

Because of the inapplicability of perturbative QCD at a scale ~ 1 GeV, the hadronisation schemes imposed after the parton production are by necessity phenomenological. The phenomenology, however, must itself be a manifestation of QCD from which we may eventually deduce a sound theory of hadronisation. However regrettable this situation may be from the point of view of theoretical physics, the fact remains that the fragmentation models provide the intermediary for the comparison of perturbative QCD

parton-level calculations with the experimentally measured hadronic final state. The task of isolating which properties of the hadronic state may be understood in terms of the underlying perturbative QCD processes, and which are influenced by the non-perturbative hadronisation mechanism, is very difficult within the context of the QCD + fragmentation models. A thorough understanding is required of the effects of the input phenomenological hadronisation scheme and the variation produced by changing the model arbitrary parameters, not to mention uncertainties in the perturbative calculations such as the value of the QCD scale parameter Λ. That unfolding all of these effects is difficult, awkward and tedious is clear, but necessary if one wishes to study QCD predictions in detail and make a more definite conclusion than merely that some models describe the data whilst others do not. These problems will become less severe only when respectable theoretical calculations of hadronisation exist, a situation which is at present unforseeable. Comparison of perturbative QCD + fragmentation models with data is hence unavoidable for testing QCD.

These models are also important for other reasons:

(i) The accurate simulation of detector response is essential to the understanding of the performance of complex particle detectors. The foundation of any such simulation must be an event generator implementing a physics model.

(ii) In experimentally analysing most known processes one needs an estimate of background contributions. Such estimates of contamination from 'standard' hadronic events are provided by QCD + fragmentation models. In particular, in looking for signatures of new processes at higher energies, which may have small cross sections, an accurate simulation of such 'standard' event properties is absolutely essential.

(iii) Most experimental measurements are unfolded from the 'raw' data to correct for the effects of detector acceptance and response. Such correction procedures require accurate Monte Carlo simulations of event properties generated using the models.

There are few papers published by experiments at high energy e^+e^- colliders which do not rely on the use of one or other of the QCD + fragmentation models at some point in the analysis.

This paper is complementary to [3], where the event characteristics in the c.m. energy range $12.0 \leqq \langle W \rangle \leqq 41.5$ GeV are described, and also to [10], which discusses the multijet structure of the data. The main emphasis of this paper is on the model predictions at higher energies. In all of these studies the following perturbative QCD + fragmentation models are used:

(i) The $O(\alpha_s^2)$ matrix elements (ME) of Gutbrod et al. [5] with hadronisation of the parton state by the Lund string model [6], incorporated into the Lund Monte Carlo JETSET version 6.3 [7].

(ii) The Webber LLA parton cascade with soft gluon interference [8] and hadronisation by the formation and decay of colourless clusters, incorporated in the Monte Carlo program BIGWIG version 4.2.

(iii) The LLA parton cascade + $O(\alpha_s)$ ME generator [9], which includes soft gluon interference effects, with Lund string hadronisation, also included in version 6.3 of the Lund Monte Carlo.

The main features of the models are described in [3, 10], in addition to the parameter tuning procedure and the selection and correction of the TASSO data also presented here.

There are several purposes to the high energy extrapolations presented in this paper.

(i) To give an idea of event characteristics at higher energies and the general physics environment within which detectors will operate. Good estimates of quantities such as particle multiplicity and momentum spectra are clearly of relevance to the design of detectors, online data processing and analysis programs. For this purpose, the differences between the model predictions in the high energy extrapolation may be taken to represent the theoretical uncertainty.

(ii) Most of the events described here involve continuum production of the five known quark flavours, and hence represent backgrounds to any new physics processes. Significant deviations from the event properties shown will be evidence for new physics.

(iii) The differences between the model results are interesting in their own right and reflect the underlying physics. In some cases the differences are so large that the data should have no difficulty in showing a preference, in contrast to the energies so far explored where all three models considered are quite successful.

2. Evolution of observables between $W = 12$ and 200 GeV

The mean values of well-known observable characteristics of hadronic event shapes and single track quantities are shown as a function of W in Figs. 1 to 6. The data cover the energy range $12.0 \leqq \langle W \rangle \leqq 41.5$ GeV, whilst the model curves (for u, d, s, c, b production only) extend up to 200 GeV. Unless otherwise stated, the errors on the TASSO data at $W = 35$ GeV

are the sum in quadrature of the statistical errors and the errors from the background subtraction and correction procedure [3]. The TASSO data at other energies are taken from [11]; the data at 29 GeV are from Mark II [2] and HRS [12]; the Mark II errors are the sum in quadrature of the statistical errors and the uncertainty in the correction procedure; the other data show statistical errors only, except where explicitly mentioned otherwise. The model parameters used, given in the Appendix, were those optimised at $W=35$ GeV as described in [3]. Note that in the high energy extrapolation, both the LLA cascade model predictions should be taken more seriously than those of the $O(\alpha_s^2)$ model. The latter has already been shown [10, 13] (see also Sect. 4) to give too few $\geqq 4$ jet events at PETRA and, by definition, cannot reproduce the multiple soft gluon emission expected in the 100 GeV energy domain.

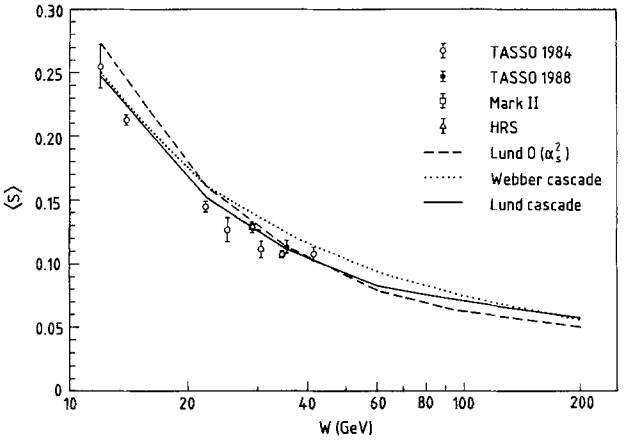

Fig. 1. The mean sphericity as a function of W for the TASSO data in the range $12 \leqq \langle W \rangle \leqq 41.5$ GeV, the HRS and Mark II data at $W=29$ GeV and for the models up to 200 GeV

For the models, the event shape observables sphericity, thrust and aplanarity were determined using both charged and neutral particles which were either prompt or produced by the decay of particles with lifetimes less than $3 \times 10^{-10} s$. The TASSO measurements of these quantities used charged particles only, and were corrected for neutral particle effects [3, 11]. All single track quantities are shown for charged particles only. The lines in the figures join the MC calculated points at $W=12$, 14, 22, 35, 60, 93, 150, 200 GeV.

The mean sphericity values are shown in Fig. 1. Interestingly the Webber cascade gives systematically more spherical events than the Lund cascade, even though the latter contains hard gluon emission to $O(\alpha_s)$ by including the $O(\alpha_s)$ ME factor. This may well be a consequence of the cluster hadronisation mechanism employed by Webber, in which colourless clusters of mass larger than M_c are split into two before they are allowed to decay by phase space. From the tuning to TASSO data at 35 GeV c.m. energy, a low value $M_c=2.3$ GeV/c^2 was obtained, which would have less effect at low W, where few clusters with mass above M_c are produced anyway, and also at high W, where the hadronic final state is dominated by the parton cascading rather than by hadronisation effects. The convergence of the Lund and Webber cascades around 12 and 200 GeV is consistent with this hypothesis, though other differences in the way the cascades are initialised and evolved [3, 14] may also contribute. Generally closer agreement between these two cascade models was obtained by Mark II in their extrapolation up to $W=93$ GeV [2], using $M_c=3.0$ GeV, though the values of other parameters were different from those used here [3]. Above 60 GeV the $O(\alpha_s^2)$ model gives fewer spherical events (Fig. 1), also reflected in higher mean thrust values

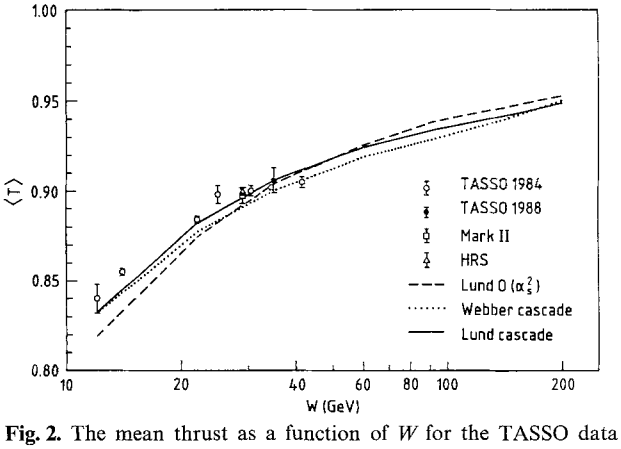

Fig. 2. The mean thrust as a function of W for the TASSO data in the range $12 \leqq \langle W \rangle \leqq 41.5$ GeV, the HRS and Mark II data at $W=29$ GeV and for the models up to 200 GeV

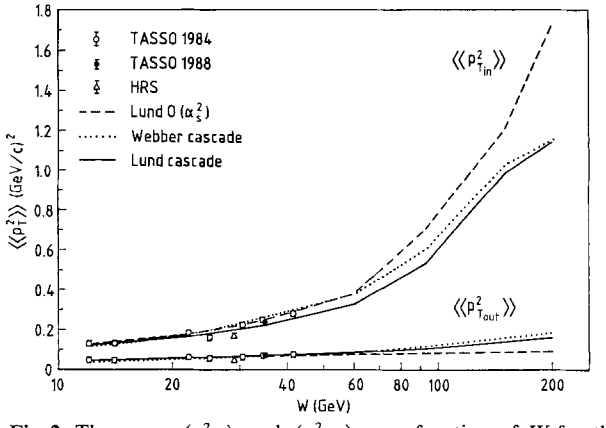

Fig. 3. The mean $\langle p_{T_{in}}^2 \rangle$ and $\langle p_{T_{out}}^2 \rangle$ as a function of W for the TASSO data in the range $12 \leqq \langle W \rangle \leqq 41.5$ GeV, the HRS data at $W=29$ GeV and for the models up to 200 GeV

(Fig. 2). Again in Fig. 2 the Lund and Webber cascades agree at low and high W, though Webber gives fewer high thrust events in between. From Fig. 1, $\langle S \rangle$ at $W=200$ GeV is predicted to be about half of the 35 GeV value, whilst $\langle T \rangle$ rises gradually from 0.9 (35 GeV) to 0.95 (200 GeV).

The $\langle\langle p^2_{T_{in}} \rangle\rangle$* and $\langle\langle p^2_{T_{out}} \rangle\rangle$ data are reasonably well described by all three models (Fig. 3), though large differences between them emerge in the high energy extrapolation: the $O(\alpha_s^2)$ model gives significantly higher $\langle\langle p^2_{T_{in}} \rangle\rangle$ than the two cascades, whilst the multiple soft gluon emission in the LLA formalism shows itself as greater $\langle\langle p^2_{T_{out}} \rangle\rangle$ relative to the $O(\alpha_s^2)$ ME.

The high energy results for single particle $\langle p_T \rangle$ (relative to the sphericity axis) are similar (Fig. 4) for all three models. $\langle p_T \rangle \sim 0.6$, 0.8 GeV/c at $W=100$, 200 GeV respectively, compared to ~ 0.4 GeV/c around $W=30$ GeV. The good agreement between the two cascade models in terms of $\langle n_{ch} \rangle$ (Fig. 5), for $W>40$ GeV, is remarkable. The data are described quite well by all models (the errors on the data include the systematic uncertainty), but above 50 GeV c.m. energy the LLA cascades give a higher multiplicity which increases faster with W: they predict about 21 charged particles per event at $W=93$ GeV, 3 units above $O(\alpha_s^2)$, and about 28 charged particles at 200 GeV, 7 units higher than $O(\alpha_s^2)$. This discrepancy becomes even larger as TeV energies are approached [15]. It is interesting that the average n_{ch} from the cascade Monte Carlos agrees well, to within roughly 10%, with the expected multiplicity evolution formula derived analytically from leading and next to-leading order QCD [16] and normalised at low energies to take the incalculable non-perturbative effects into account.

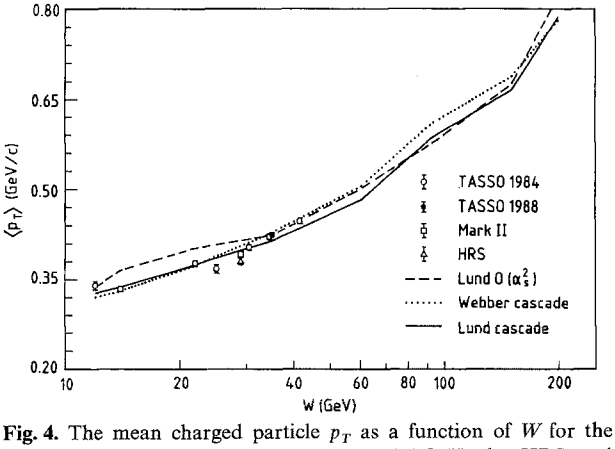

Fig. 4. The mean charged particle p_T as a function of W for the TASSO data in the range $12 \leqq \langle W \rangle \leqq 41.5$ GeV, the HRS and Mark II data at $W=29$ GeV and for the models up to 200 GeV

* The inner $\langle\ \rangle$ denotes averaging over all particles in an event and the outer $\langle\ \rangle$ denotes averaging over all events

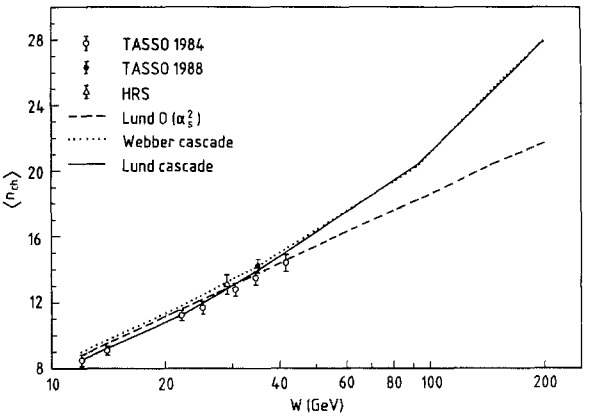

Fig. 5. The mean charged multiplicity as a function of W for the TASSO data in the range $12 \leqq \langle W \rangle \leqq 41.5$ GeV, the HRS data at $W=29$ GeV and for the models up to 200 GeV. The errors on the data include systematic effects

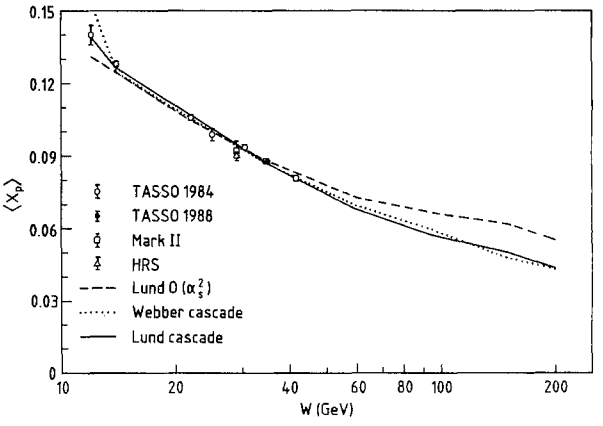

Fig. 6. The mean charged particle x_p as a function of W for the TASSO data in the range $12 \leqq \langle W \rangle \leqq 41.5$ GeV, the HRS and Mark II data at $W=29$ GeV and for the models up to 200 GeV

Differences between the cascade models and the $O(\alpha_s^2)$ model are further evident in the behaviour of mean particle $x_p = 2p/W$ (Fig. 6), where the hard tail at high W for the latter is a consequence of the fragmentation of a small number of hard partons, whereas the emission of many soft partons in the LLA cascades has an overall softening effect on the particle momentum spectrum of the hadronic final state. At $W=93$ GeV the typical charged particle momentum is ~ 2.7, 3.1 GeV/c for the LLA cascades and $O(\alpha_s^2)$ models respectively.

3 Differential distributions at higher energies

From Figs. 1–6 it can be seen that the energy evolution of the mean values of the observables in the data is reasonably well described by all the models, and

that differences between them subsequently appear at higher energies. The actual differential distributions are shown in Figs. 7–17 at the Z^0 energy, $W=93$ GeV, for u, d, s, c, b events generated with all three models, as well as for comparison the TASSO 1986 35 GeV data to illustrate how the distributions change with energy. For the sake of clarity, only the Lund cascade prediction is shown at 200 GeV as an additional curve; this model was found [2, 3] to give the best overall description of the 35 GeV data, as well as the energy evolution of the mean values in the range $12.0 \leqq \langle W \rangle \leqq 41.5$ GeV. The effect of top quark production on the global properties of the hadronic final state at $W=200$ GeV is illustrated for several quantities for the case $m_{\text{top}}=60$ GeV/c^2, where $u, d, s, c, b+t$ production was simulated using the Lund cascade*. For the models the lines in the figures join the MC calculated joints.

Similar sphericity distributions at 93 GeV (Fig. 7) are given by all models; the decrease in the number of spherical events as W increases is apparent. Including t quark production does give more spherical events, though for the sake of clarity this is not shown in the figure. The difference in aplanarity between the $O(\alpha_s^2)$ ME and the two cascades is huge at 93 GeV (Fig. 8), though the Lund cascase itself gives fewer events than Webber at high A. Because of the inherent high transverse momentum of top hadron decay products, top quark production gives rise to many aplanar events, illustrated dramatically in Fig. 8. Similar differences in thrust are observed at 93 GeV (Fig. 9) as at 35 GeV [3]; low thrust events are somewhat suppressed in the $O(\alpha_s^2)$ model whilst Webber gives more of these events than the Lund cascade and correspondingly fewer in the peak around $T=0.96$. Top quark production gives rise to an excess of events around $T\sim 0.8$ and a suppressed rate of collimated events ($T\sim 1$) compared to u, d, s, c, b only (Fig. 9).

At $W=93$ GeV the $O(\alpha_s^2)$ model gives more very low $\langle p_{T_{\text{in}}}^2 \rangle$ events than the cascades (Fig. 10), though fewer around 0.2–0.6 (GeV/c)^2. The main differences are hence in the low p_T region rather than the high p_T tail. The large discrepancies between models seen in aplanarity are reflected in $\langle p_{T_{\text{out}}}^2 \rangle$ (Fig. 11) where the $O(\alpha_s^2)$ distribution is shifted towards low p_T, and $p_{T_{\text{out}}}$ (Fig. 13); the differences between Lund and Webber cascades are large at 93 GeV. Both $\langle p_{T_{\text{in}}}^2 \rangle$ and

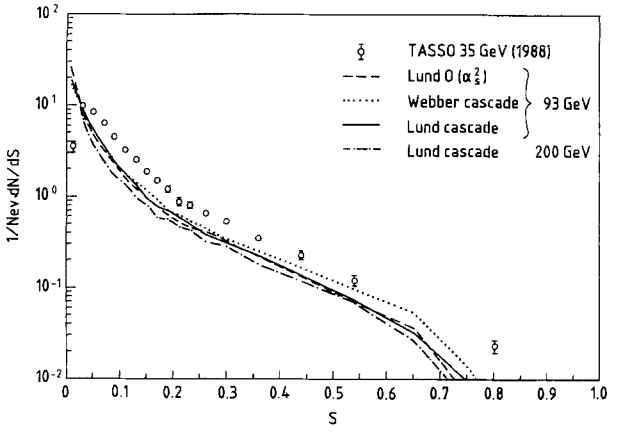

Fig. 7. The sphericity distribution for the models at $W=93$ GeV and 200 GeV; the TASSO data at 35 GeV are shown for comparison

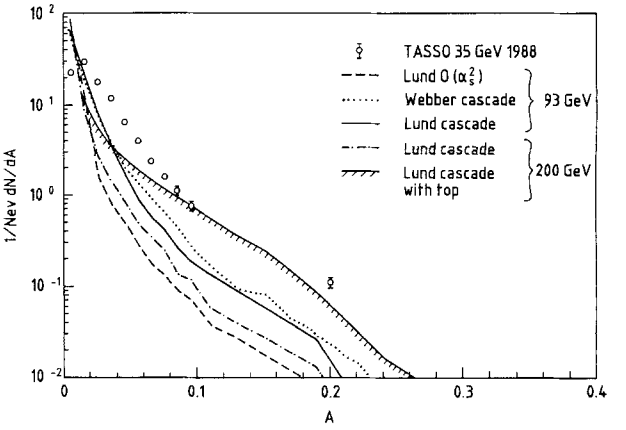

Fig. 8. The aplanarity distribution for the models at $W=93$ GeV and 200 GeV; the TASSO data at 35 GeV are shown for comparison

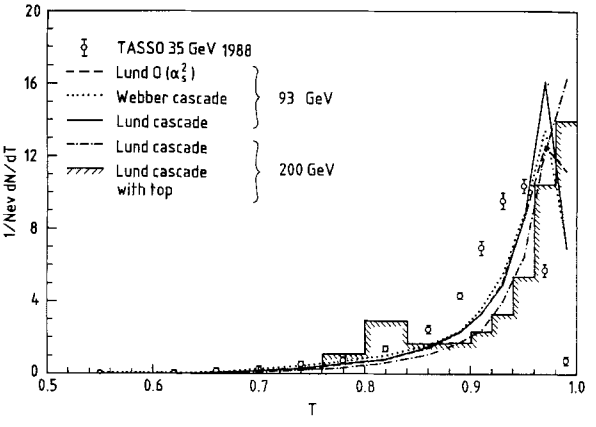

Fig. 9. The thrust distribution for the models at $W=93$ GeV and 200 GeV; the TASSO data at 35 GeV are shown for comparison. (The Lund cascade model prediction including top production at $W=200$ GeV is shown as a histogram for the sake of clarity)

* After string fragmentation of the parton state, weak decays of top hadrons are treated according to the spectator model. The decay products are distributed according to the standard $V-A$ matrix elements. In most cases the spectator quark system and the $q\bar{q}$ system from the W are each fragmented separately by connecting a Lung string between the two quarks, although the other possibility of a rearrangement of the colour singlet systems via a soft gluon exchange is also taken into account [17]

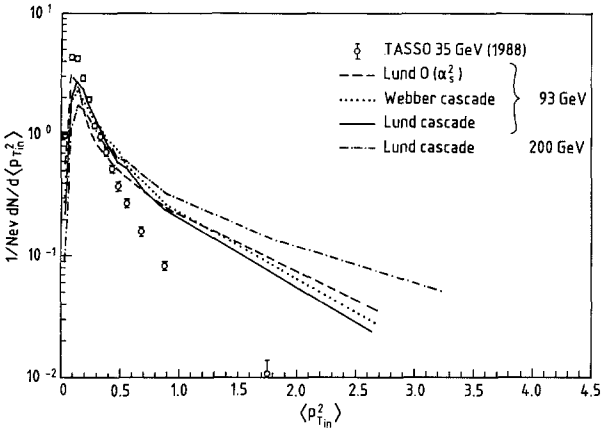

Fig. 10. The $\langle p_{T_{in}}^2 \rangle$ distribution for the models at $W=93$ GeV and 200 GeV; the TASSO data at 35 GeV are shown for comparison

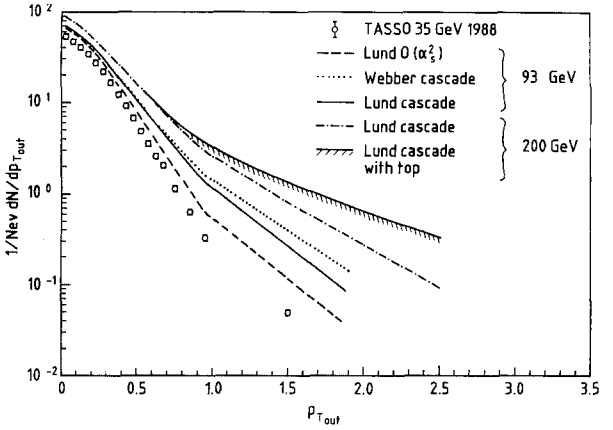

Fig. 13. The $p_{T_{out}}$ distribution for the models at $W=93$ GeV and 200 GeV; the TASSO data at 35 GeV are shown for comparison

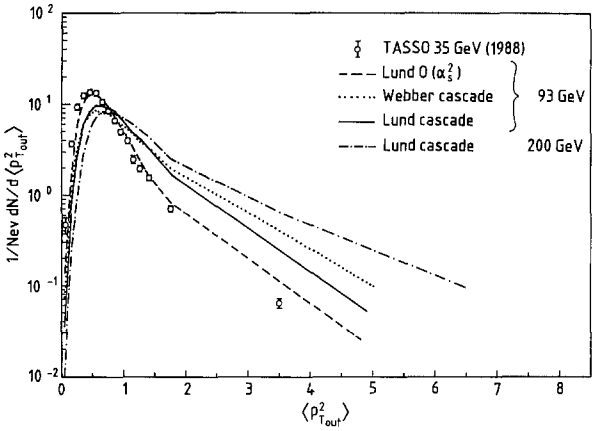

Fig. 11. The $\langle p_{T_{out}}^2 \rangle$ distribution for the models at $W=93$ GeV and 200 GeV; the TASSO data at 35 GeV are shwon for comparison

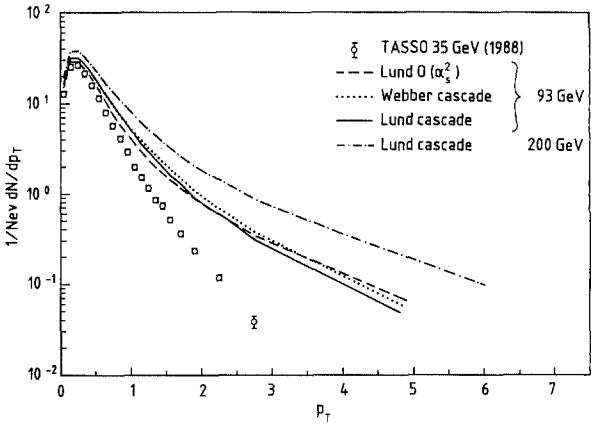

Fig. 14. The p_T distribution for the models at $W=93$ GeV and 200 GeV; the TASSO data at 35 GeV are shown for comparison

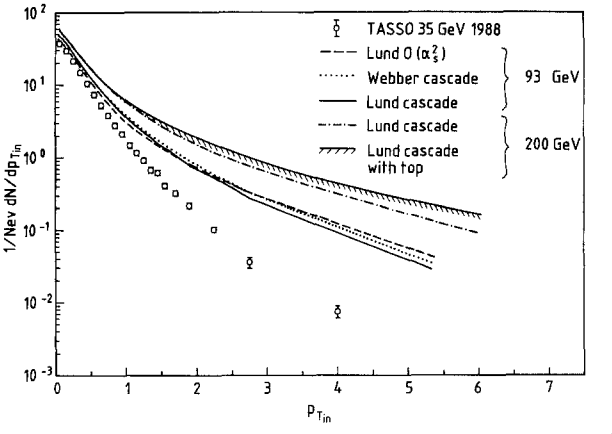

Fig. 12. The $p_{T_{in}}$ distribution for the models at $W=93$ GeV and 200 GeV; the TASSO data at 35 GeV are shown for comparison

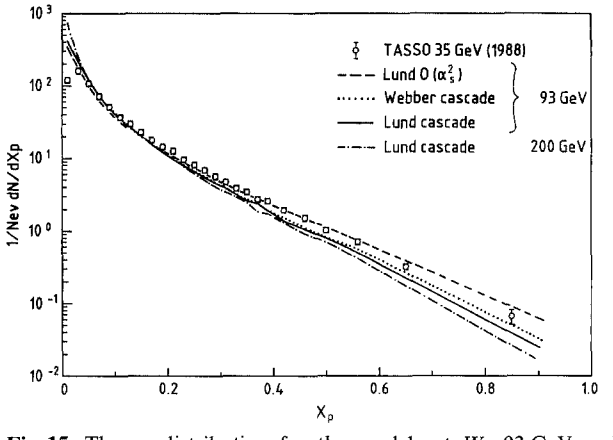

Fig. 15. The x_p distribution for the models at $W=93$ GeV and 200 GeV; the TASSO data at 35 GeV are shown for comparison

$\langle p_{T_{out}}^2 \rangle$ are relatively insensitive to top production (not shown). The $p_{T_{in}}$ and p_T distributions (Figs. 12, 14 respectively) are rather similar for all models at 93 GeV; a significant high momentum tail develops at 200 GeV, further emphasised by the higher particle multiplicity. Greater numbers of tracks of high $p_{T_{in}}$ and $p_{T_{out}}$ are evident for top production in Figs. 12, 13.

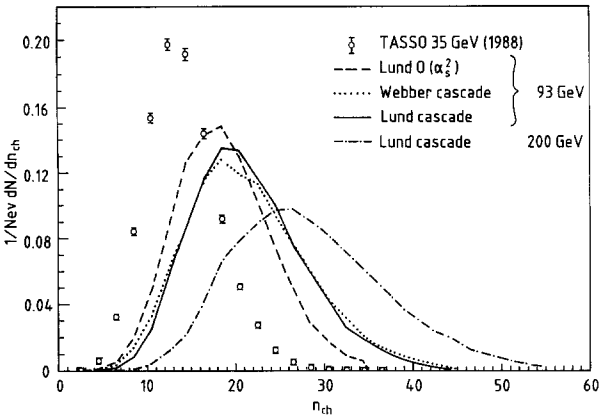

Fig. 16. The charged particle multiplicity distribution for the models at $W=93$ GeV and 200 GeV; the TASSO data at 35 GeV are shown for comparison

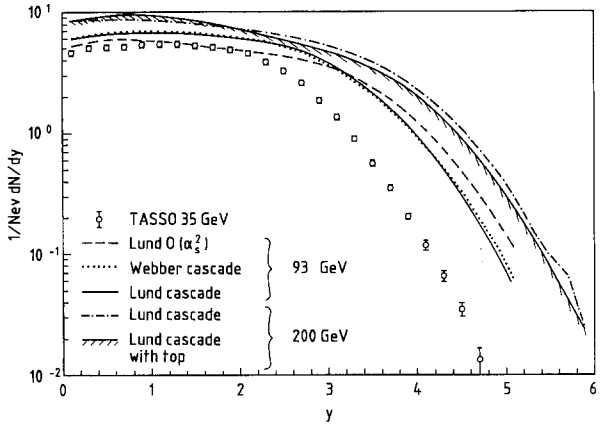

Fig. 17. The charged particle rapidity (with respect to the thrust axis) distribution for the models at $W=93$ GeV and 200 GeV; the TASSO data at 35 GeV are shown for comparison

Bearing in mind that at 93 GeV the $O(\alpha_s^2)$ model has a lower charged multiplicity by three units, its very hard x_p spectrum (Fig. 15) relative to the cascades is a striking consequence of the absence of multiple gluon bremsstrahlung. Charged particle multiplicity distributions are shown in Fig. 16, where in addition to higher mean values the cascade models also have larger dispersions at 93 GeV than the $O(\alpha_s^2)$ model. The Lund cascade distribution at 200 GeV is very broad, with a long tail extending beyond 50 charged particles per event. At $W=93$ GeV the smaller $O(\alpha_s^2)$ particle multiplicity is reflected in a lower rapidity plateau (Fig. 17), though this model gives more particles at high y, in comparison to the rather similar distributions for the two cascades. Inclusion of top production is illustrated in Fig. 17, where an excess of tracks around $y\sim 1$ reflects the intrinsic high p_T of top hadron decay products. There is no appreciable change in particle multiplicity or momentum (x_p) distributions at $W=200$ GeV with the top quark included (not shown).

4 Jet multiplicities

The jet structure of hadronic events in e^+e^- annihilation is interesting not only in its own right as a reflection of the underlying parton production, but also at high c.m. energies as a background to other processes which give rise to multijet final states, such as $e^+e^-\to W^+W^-$ (see e.g. [18]). Detailed studies of multijet production using a cluster algorithm for jet finding have been performed at PETRA [10, 13] and also in studies for e^+e^- collisions at higher energies [19] and for ep interactions at the HERA collider [20] currently under construction.

A brief description of the cluster algorithm is now given; further details many be found in [10, 13]. The invariant mass-squared m_{ij}^2 is calculated for all pairs of particles i,j in an event according to the formula:

$$m_{ij}^2=2E_iE_j(1-\cos\theta_{ij})$$

where all particles are assumed to have the pion mass. The pair with the lowest m^2 are combined into a 'pseudoparticle' by adding their momentum 4-vectors. The procedure is repeated, the pair with the lowest m^2 being combined each time, until all remaining pseudoparticle pairs have invariant masses which satisfy:

$$m_{ij}^2>m_{ij}^{\mathrm{cut}^2}$$

where m_{ij}^{cut} is an arbitrary jet resolution parameter. From PETRA experience $m_{ij}^{\mathrm{cut}}=7$ GeV/c^2 is a reasonable value and allows comparison of these results with those of the other studies [10, 13, 19, 20]. This value is used here unless stated otherwise.

The resulting jet multiplicities are shown for the Lund $O(\alpha_s^2)$ ME model in Fig. 18a and for the Webber ('LLA model') and Lund ('LLA+$O(\alpha_s)$ model') cascades in Fig. 18b. Also shown are the TASSO data from [10], which were fully corrected for detector effects and initial state radiation. Both charged and neutral particles were used in the MC calculations as described in Sect. 2; the lines in the figures join the MC calculated points at c.m. energies of 14, 22, 35, 44, 60, 93 and 200 GeV.

The $O(\alpha_s^2)$ ME model gives too few 4, 5-jet events compared with the TASSO data, though the rates of 2, 3-jet events are well described (Fig. 18a). The need for perturbative QCD contributions of order higher than α_s^2 to describe the multijet rates is hence already observable at PETRA energies. Therefore the 4, 5-jet rates at higher c.m. energies are expected to be seriously underestimated by this model, which by definition allows production of up to a maximum of 4 partons. Note however that above 60 GeV the 2, 3-jet rates decrease only very slowly with energy, imply-

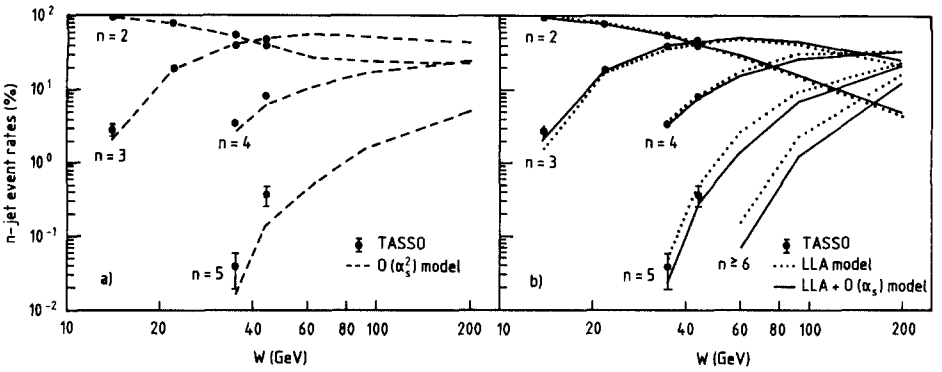

Fig. 18a, b. The rates of n-jet events observed in the TASSO data and the perturbative QCD+fragmentation models: **a** Lund $O(\alpha_s^2)$ ME calculations, **b** Webber LLA cascade and Lund LLA cascade $+O(\alpha_s)$ ME calculations

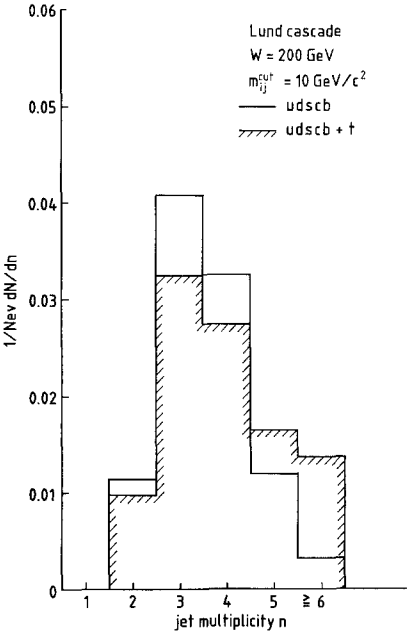

Fig. 19. The jet multiplicity distribution for the Lund cascade model at $W=200$ GeV for jet mass-resolution $m_{ij}^{\text{cut}}=10$ GeV/c^2

ing both that the parton jet structure is fully resolved after hadronisation and that hadronisation fluctuations do not give rise to many spurious jets. The 5-jet events in Fig. 18a must be due to such fluctuations and represent about 2% (5%) of all events at $W=93$ (200) GeV.

The Webber cascade slightly overestimates and underestimates respectively the 2, 3-jet rates in the TASSO data, though is in good agreement with the observed 4, 5-jet rates (Fig. 18b). The Lund cascade represents all jet rates in the data well. (See [10] for a more detailed discussion.) These model calculations at higher W should therefore be taken seriously; the difference between the Webber and Lund calculations provides an estimate of the theoretical uncertainty in the extrapolation. The total jet cross section at $W=200$ GeV is dominated by $\geqq$4-jet final states, which will form a background to events containing heavy states which decay into hadron jets. In particular events of the type $e^+e^-\to W^+W^-$, where each W decays to two quarks, may be difficult to isolate as gluon bremsstrahlung from the quarks disrupts the simple four jet event topology. It is estimated [18] that 43% (40%) of W^+W^- events will give rise to 5 ($\geqq$6) resolvable partons, and hence in principle up to 5 or 6 hadron jets.

Jet rates at $W=200$ GeV are shown in Table 1 with and without top quark production, and for two values of the jet mass resolution $m_{ij}^{\text{cut}}=7$ and 10 GeV/c^2. (The errors shown are statistical). Note that all stable particles were used in the jet finding. The second case is also shown in Fig. 19. Clearly events containing top quarks give on average more jets than those of the lighter flavours. This is a further reflection of the relative high transverse momentum of the top hadron decay products resulting from the large top mass, such that, together with hadronisation fluctuation effects, more clusters are found by the algorithm.

Table 1

Rate of n-jet events (%)		2	3	4	5	≧6
$m_{ij}^{\text{cut}}=7$ GeV/c^2	u, d, s, c, b	5.25±0.22	26.62±0.50	34.43±0.57	21.87±0.45	11.84±0.33
	$+t$	4.46±0.17	22.06±0.37	28.09±0.42	20.88±0.36	24.51±0.39
$m_{ij}^{\text{cut}}=10$ GeV/c^2	u, d, s, c, b	11.39±0.26	40.80±0.50	32.66±0.45	11.88±0.27	3.28±0.14
	$+t$	9.80±0.25	32.52±0.45	27.39±0.41	16.64±0.32	13.65±0.29

5 Summary and conclusions

The three most successful perturbative QCD+fragmentation models have been analysed at c.m. energies between 12 and 200 GeV. The few most important parameters of each model had been optimised to provide a good description of the features of the high statistics data sample collected by TASSO at 35 GeV. All the models reproduce reasonably well the evolution of the mean values of observables in the data as a function of c.m. energy in the range $12 \leqq \langle W \rangle \leqq 41.5$ GeV, though differences between model predictions subsequently appear at higher energies. For some quantities, e.g. $\langle\langle p^2_{T_{\text{out}}}\rangle\rangle$, $\langle n_{\text{ch}}\rangle$, $\langle x_p\rangle$, the differences are extremely large above about 60 GeV, so that the data to be collected at the forthcoming e^+e^- colliders in the 100 GeV energy range should easily be able to discriminate between models.

Large differences between models at $W=93$ GeV are also seen in the differential distributions of quantities such as aplanarity, thrust and $p_{T_{\text{out}}}$, though for other variables, such as sphericity and $p_{T_{\text{in}}}$, the differences are smaller, providing a less sensitive test of the models. The Lund cascade was generally the most successful at representing the PETRA/PEP data [2, 3] so that results were also shown for this model at $W=200$ GeV in order to get some idea of the hadronic final state properties, though clearly an extrapolation to 200 GeV using model parameters extracted at 35 GeV should not be regarded as anything other than a reasonable estimate.

The inclusion of top quark production at $W=200$ GeV was simulated using the Lund cascade for $m_{\text{top}}=60$ GeV/c^2. Of the event shape observables, the aplanarity and thrust distributions appear to be particularly sensitive to the presence of the top quark events. Kinematic effects in top hadron decay appear as an excess of particles at high $p_{T_{\text{in}}}$ and $p_{T_{\text{out}}}$ and around a rapidity of 1.

From experience of comparing the models with data at PETRA and PEP, where no one model accurately describes every quantity presented here at a single centre of mass energy, e.g. 29 GeV [2] or 35 GeV [3], let alone across the full energy range already explored [2, 3], it is clear that to describe additionally data around 100 GeV or higher, with parameters which are fixed for all energies, will prove a challenging test of the QCD+fragmentation models.

Acknowledgements. I would like to thank M. Bengtsson, M.G. Bowler, G. Ingelman, D.H. Saxon, T. Sjöstrand and B.R. Webber for helpful discussions, and the members of the TASSO Collaboration for their support and assistance. This work was supported in part by the U.K. Science and Engineering Research Council.

Appendix: model parameters optimised at $W=35$ GeV

Any parameters not mentioned below were left at their default values.

Parameters for the Webber cascade model

Λ_{LL} is the QCD scale parameter used in the LLA parton cascade calculations. Q_0 is the parton virtuality scale at which the cascade is terminated and partons are put on mass shell prior to the formation of colourless clusters. After heavy flavoured quarks are decayed, clusters whose mass exceeds M_c are split into two before all clusters are decayed by phase space.

Parameter	Tuned value
QCD LLA scale Λ_{LL} (GeV)	0.25
Cascade virtuality cutoff Q_0 (GeV)	0.61
Cluster-mass parameter M_c (GeV/c^2)	2.3

Parameters for the Lund cascade model

Λ_{LL} and Q_0 have the same meaning as for the Webber model. After the parton production a colour triplet string is stretched between the partons and fragmented according to the Lund recipe using the function:

$$f(z)=\frac{1}{z}(1-z)^a \exp\left(-\frac{b m_T^2}{z}\right)$$

where a, b are parameters, for all quark flavours. ($m_T^2=p_T^2+m^2$ is the hadron transverse mass-squared). σ is the width of the Gaussian p_T spectrum for primary quarks $\sim e^{-p_T^2/2\sigma^2}$. The other string fragmentation parameters, such as the strange quark- and various diquark-suppression factors, are of secondary importance to the inclusive global properties of hadronic final states and were left at their default values.

Parameter	Tuned value
QCD LLA scale Λ_{LL} (GeV)	0.26
Cascade virtuality cutoff Q_0 (GeV)	1.0
Fragmentation function parameter a	0.18
Fragmentation function parameter b	0.34
Gaussian p_T parameter $\sqrt{2}\sigma$ (GeV/c)	0.39

Parameters for the Lund $O(\alpha_s^2)$ model

$\Lambda_{\overline{MS}}$ is the QCD scale parameter for the second order matrix element calculations of the partonic state*. Hadronisation by the Lund string scheme involves the parameters a, b, σ as discussed above.

Parameter	Tuned value
QCD scale in $O(\alpha_s^2)$ $\Lambda_{\overline{MS}}$ (GeV)	0.62
Fragmentation function parameter a	0.58
Fragmentation function parameter b	0.41
Gaussian p_T parameter $\sqrt{2\sigma}$ (GeV/c)	0.40

References

1. For a general review see T. Sjöstrand: Int. J. Mod. Phys. A3 (1988) 751
2. Mark II Coll. A. Petersen et al.: Phys. Rev. D37 (1988) 1
3. TASSO Coll. W. Braunschweig et al.: Oxford Nuclear Physics 42/88 (1988)
4. VENUS Coll. H. Yoshida et al.: Phys. Lett. 198B (1987) 570; AMY Coll. H. Sagawa et al.: Phys. Rev. Lett. 60 (1988) 93; TOPAZ Coll. I. Adachi et al.: Phys. Rev. Lett. 60 (1988) 97
5. F. Gutbrod, G. Kramer, G. Schierholz: Z. Phys. C – Particles and Fields 21 (1984) 235
6. B. Andersson, G. Gustafson, G. Ingelman, T. Sjöstrand: Phys. Rep. 97 (1983) 33
7. T. Sjöstrand, M. Bengtsson: Comput. Phys. Commun. 43 (1987) 367
8. G. Marchesini, B.R. Webber: Nucl. Phys. B238 (1984) 1; B.R. Webber: Nucl. Phys. B238 (1984) 492
9. M. Bengtsson, T. Sjöstrand: Phys. Lett. 185B (1987) 435
10. TASSO Coll. W. Braunschweig et al.: Oxford Nuclear Physics 29/88 and DESY 88-046 (1988)
11. TASSO Coll. M. Althoff et al.: Z. Phys. C – Particles and Fields 22 (1984) 307
12. HRS Coll. D. Bender et al.: Phys. Rev. D31 (1985) 1
13. JADE Coll. W. Bartel et al.: Z. Phys. C – Particles and Fields 33 (1986) 23
14. P. Dauncey, Oxford D. Phil Thesis, RAL T 034 (1986)
15. P.N. Burrows, G. Ingelman: Z. Phys. C – Particles and Fields 34 (1987) 91
16. B.R. Webber: Phys. Lett. 143B (1984) 501
17. T. Sjöstrand: Lund preprint LU TP 85-10 (1985)
18. P. Mättig, M. Dittmar: Z. Phys. C – Particles and Fields 35 (1987) 221
19. G. Marchesini, B.R. Webber, Cavendish-HEP-87/2 (1987)
20. P.N. Burrows, G. Ingelman, E. Ros: Z. Phys. C – Particles and Fields 39 (1988) 257
21. G. Kramer, B. Lampe: DESY 86–119 (1986)

* In these calculations two partons are resolvable provided their invariant mass-squared exceeds $y_{\min} \times s$ [21]; the default value $y_{\min} = 0.02$ was used